Available online at www.sciencedirect.com
SCIENCE DIRECT
Thermochimica Acta 439 (2005) 74–79
thermochimica acta
www.elsevier.com/locate/tca

Evaluation of porous structure of resorcinol-formaldehyde hydrogels by thermoporometry

T. Yamamoto [a,*], S.R. Mukai [b], K. Nitta [b], H. Tamon [b], A. Endo [a], T. Ohmori [a], M. Nakaiwa [a]

[a] *National Institute of Advanced Industrial Science and Technology (AIST), Central 5, 1-1-1 Higashi, Tsukuba, Ibaraki 305-8565, Japan*
[b] *Department of Chemical Engineering, Kyoto University, Katsura, Nishikyo-ku, Kyoto 615-8510, Japan*

Received 26 May 2005; received in revised form 4 September 2005; accepted 10 September 2005
Available online 13 October 2005

Abstract

The porous structures of resorcinol-formaldehyde (RF) hydrogels were evaluated by thermoporometry (TPM) based on the thermodynamic relationship between the size of the pores and the solidification temperature of the freezable pore water in the pores. Adding the thickness of the nonfreezable pore water layer to the ice crystal size distribution of the freezable pore water calculated from the thermogram (a recording of the heat flux during the solidification of the freezable pore water) allowed for the determination of the porous properties of the RF hydrogels. It was confirmed that the RF hydrogels possess a fairly uniform mesoporous structure formed between the interconnected primary particles, and that the size of the mesopores clearly increased with the increase in the molar ratio of resorcinol to catalyst (*R*/*C*) used in the preparation of the initial RF solution. The dependence of both the mesopore volume and the surface area of a given RF hydrogel on the *R*/*C* ratio were also established.

Keywords: DSC; Mesoporosity; Pore size distribution; RF hydrogel; Thermoporometry

1. Introduction

A sol–gel polycondensation of metal alkoxides yields a transparent hydrogel that possesses a structure composed of a three-dimensional network that arises from interconnecting primary particles. If such a hydrogel is dried under supercritical conditions so as to maintain the network structure, a highly porous solid, called an aerogel, can be obtained. The most common inorganic aerogel is a silica aerogel [1]. The numerous potential industrial applications of these materials, including adsorbents, column-packing materials for HPLC, and supporting materials for catalysts, has led to the synthesis of various aerogels and related porous materials during the last two decades. An organic aerogel can also be synthesized by the sol–gel polycondensation of, for example, resorcinol with formaldehyde under slightly basic aqueous conditions followed by supercritical drying with carbon dioxide [2–4]. Resorcinol-formaldehyde (RF) organic aerogels are useful precursors of carbon aerogels, which can be prepared by pyrolyzing an RF aerogel in an inert atmosphere [2–4].

The key to the success of aerogels in the above applications is their mesoporosity. Achieving the desired mesoporosity in RF aerogels has been the focus of the majority of the research in this area [4,5]. RF aerogels have been used as a standard material to study the relationship between synthetic conditions and mesoporosity. However, the porous structure of an RF aerogel is not the same as that of the original hydrogel, since the shrinkage of the mesopores during supercritical drying is not negligible. Therefore, it is necessary to assess the porous structure of RF hydrogels as synthesized to understand and control the mesoporosity of the resulting RF aerogels more precisely. Although the authors have previously studied the structure formation of RF hydrogels during the sol–gel polycondensation of resorcinol with formaldehyde using scattering techniques (SAXS, DLS, and SLS) [6,7], the porous structure of the RF hydrogels could not be assessed, and has yet to be reported. As a result, the relationship between the conditions of the sol–gel polycondensation and the mesoporosity of the RF hydrogels has not yet been clarified.

Thermoporometry (TPM) is a suitable method for studying the structure of a porous solid immersed in a fluid based on the thermodynamic relationship between the pore size and the temperatures at which freezing or melting of the fluid in the pores occurs. This relationship allows for the determination of the pore

* Corresponding author. Tel.: +81 298 61 7896; fax: +81 298 61 4660.
E-mail address: yamamoto-t@aist.go.jp (T. Yamamoto).

0040-6031/$ – see front matter © 2005 Elsevier B.V. All rights reserved.
doi:10.1016/j.tca.2005.09.010

size, pore volume, pore shape, and the internal surface area of a wet solid before drying. During the last two decades, TPM has been used to characterize various porous materials. Quinson et al. measured the pore-size distribution of a silica gel and a titanium gel synthesized by the hydrolysis and sol–gel polycondensation of metal alkoxides and determined the parameters for controlling the porous structures [8–10]. Ishikiriyama et al. evaluated the pore-size distribution, the shape factor, and the internal surface area of a series of silicas with different pore radii in the range of 2–30 nm [11–13]. The influence of drying on the porous properties of hydrothermally-aged silica hydrogels was studied by Titulaer et al. [14,15]. Wulff conducted TPM studies using acetonitrile as an alternative pore-filling solvent [16]. Recently, ordered mesoporous silicas such as MCM-41, FSM-16, and SBA-15 were synthesized using spontaneously formed surfactant micelles as structure-directing agents [17–19]. The well-defined structure of these mesoporous silicas has confirmed the accuracy of TPM in the characterization of various mesoporous materials. Denoyel et al. examined the melting and freezing of water in a series of ordered mesoporous silicas with different pore sizes and obtained an empirical relationship between the pore-shape factor and the radius of the mesopores [20]. The authors also evaluated the accuracy of TPM in determination of the mesoporosity of SBA-15 [21]. Based on the above results, TPM has been confirmed to be a useful and reliable method in determining the mesoporosity of wet porous solids.

In the present study, thermograms during the freezing and melting of the water contained in RF hydrogels were acquired using differential scanning calorimetry (DSC). The porous properties of various RF hydrogels were determined by adding the thickness of the nonfreezable pore water layer to the ice crystal size distribution of the freezable pore water obtained from the freezing thermogram. Using this data, the relationship between the amount of basic catalyst used in the sol–gel polycondensation and the resulting mesoporosity of the RF hydrogels was clarified.

2. Theoretical

Based on the model depicted in Fig. 1, pore water can be classified into two types; freezable pore water that undergoes fusion or solidification upon heating or cooling, and nonfreezable pore water that does not undergo a phase transition due to strong interactions with the pore surface. Hence, the radius of the mesopores, R_p, can be estimated from the radius of the ice crystals from the freezable pore water and the thickness of the layer of nonfreezable pore water, t_{nf}:

$$R_p = R_n + t_{nf}. \tag{1}$$

It was reported that the thickness of the layer of the adsorbed water on the silica surfaces is between 0.4 and 1.2 nm [9,13,22], which corresponds to 2–4 layers of water molecules based on the Lennard-Jones dimension of a water molecule (0.27 nm). Here, the thickness of this layer can be evaluated from the mass of the nonfreezable pore water per mass unit of dry sample, W_{nf}, according to the following equation:

$$t_{nf} = \frac{W_{nf}}{\rho_{nf} S_{BET}} \tag{2}$$

where ρ_{nf} is the density of the nonfreezable pore water, which is approximately equivalent to the density of bulk ice at 273 K (0.917×10^3 kg/m^3) [13].

The size distributions of ice crystals of the freezable pore water formed in the pores can be obtained by adopting the following equation to the thermogram:

$$\frac{dV_n}{dR_n} = \frac{dq}{dt}\frac{dt}{dT}\frac{dT}{dR_n}\frac{1}{\rho(T)\Delta H(T)m} \tag{3}$$

where V_n, dq/dt, and dt/dT represent the volume of an ice crystal, the heat flow, and the reciprocal of the rate of cooling or heating, respectively. $\rho(T)$ and $\Delta H(T)$ denote the density and the enthalpy change of the freezable pore water, respectively, both of which depend on the temperature as follows [13]:

$$\rho(T) = 0.917 \times (1.03 - 1.17 \times 10^{-4} T) \tag{4}$$

$$\Delta H(T) = 334 + 2.12 \times (T - 273) - 0.00783 \times (T - 273)^2 \tag{5}$$

Brun et al. empirically obtained a relationship between the size of an ice crystal and the freezing temperature depression of the freezable pore water, $T_0 - T$, expressed by the following equation [8]:

$$R_n = \frac{64.7}{T_0 - T} - 0.230 \tag{6}$$

Since Eqs. (4)–(6) are proposed for freezable pore water in a cooling period, the size distribution of the ice crystals is calculated by adopting the equations to the solidification thermogram. By taking both the thickness of the layer of nonfreezable water and the shape of the pore into account, the pore size distribution can be obtained as follows:

$$\frac{dV_p}{dR_p} = \frac{dq}{dt}\frac{dt}{dT}\frac{dT}{dR_p}\frac{1}{\rho(T)\Delta H(T)m}\left(\frac{R_p}{R_n}\right)^f \tag{7}$$

where the exponent f can be interpreted as the geometrical dimension of the pore. The value of f is 2 for cylindrical pores and 3 for spherical pores. Titulaer et al. proposed the following

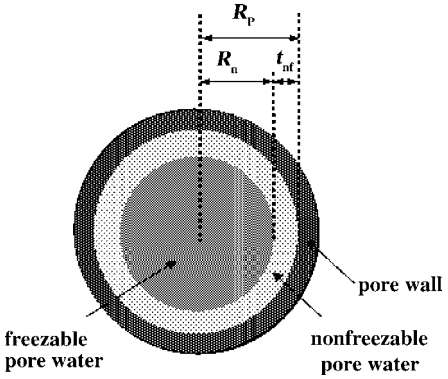

Fig. 1. Model of the types of pore water.

empirical equation to determine the value of f [15]:

$$f = 1 + \frac{2}{F} \tag{8}$$

Here, F can be experimentally determined from the peak temperature of the solidification curve, T_s, and that of the fusion curve, T_f, in the thermograms by:

$$F = \frac{T_0 - T_s}{T_0 - T_f} \tag{9}$$

The pore volume, V_p, is obtained by taking into account the layer of the nonfreezable pore water, and can be expressed by the following equation:

$$V_p = V_n \left(\frac{R_n + t_{nf}}{R_n} \right)^f \tag{10}$$

where V_n is calculated by the integration of Eq. (3).

The surface area of an ice crystal, S_n, formed in the pores can be calculated by using the following equation:

$$S_n = V_n \frac{dS_n}{dV_n} = V_n \frac{f}{R_n} \tag{11}$$

The surface area of the pores, S_p, can be estimated by the following equation:

$$S_p = S_n \left(\frac{R_n + t_{nf}}{R_n} \right)^{f-1} \tag{12}$$

3. Experimental

3.1. Synthesis of RF hydrogels and RF cryogels

RF hydrogels were synthesized from resorcinol (R) (Wako Pure Chemical Industries, research grade), formaldehyde (F) (Wako Pure Chemical Industries, research grade, 37 wt.%; formaldehyde stabilized with 8 wt.% methanol aqueous solution), sodium carbonate (C) (Wako Pure Chemical Industries, research grade), and distilled water after deionization (W). Here, sodium carbonate was used as the basic catalyst for the sol–gel polycondensation. The molar ratio of resorcinol to catalyst (R/C) was varied in the range of 200–600 mol/mol, while the molar ratio of resorcinol to formaldehyde (R/F) and the ratio of resorcinol to water (R/W) were fixed to 0.5 mol/mol and 500 kg/m^3, respectively. The solution was poured into glass tubes (inner diameter, 4 mm; length, 40 mm) and gelled by curing at 298 K for 24 h, at 323 K for 24 h, and finally at 363 K for 72 h to obtain an RF hydrogel. The RF hydrogels synthesized are referred to as RF-200, RF-400, and RF-600, where the number indicates the R/C value.

The freeze-drying of an RF hydrogel was conducted by holding the hydrogel at 243 K for 6 h and subsequently at 263 K for 24 h under vacuum to obtain an RF cryogel.

3.2. SEM observation

The cross sections of an RF cryogel and a silica gel (Q-30) (Fuji Silysia Chem. Ltd.) were observed using an SEM (JEOL; JSM-6340FS).

3.3. Adsorption measurement of N_2

The adsorption and desorption isotherms of N_2 on the RF cryogels were measured at 77 K using an automatic gas adsorption-desorption apparatus (BEL Japan; Belsorp28-SA). The BET surface area, S_{BET}, was estimated by applying the BET equation to the isotherm. In this article, the IUPAC definition of mesopores (r_p = 1–25 nm) is applied.

3.4. DSC measurement

Prior to the DSC measurements, the synthesized RF hydrogels were immersed in 20-times their volume of pure water (Wako Pure Chemical Industries, research grade) and stirred at 298 K for 24 h to remove the residual reactants and exchange the solvent filling the pores with pure water. This rinse was repeated more than seven times. The prepared samples were then sealed into an aluminum vessel. The thermograms of the water in the vessel were measured by using a differential scanning microcalorimeter (Shimadzu; DSC-60) equipped with a cooling apparatus. The vessel also contained a small amount of bulk water. Prior to measurement, the vessel was kept at 248 K. It was heated to 272 K, which is just below the melting point of bulk water. The measurement was conducted by cooling the vessel to 248 K again followed by heating to 276 K, which is above the melting temperature of the bulk water. All of the measurements were conducted using a sufficiently low cooling and heating rate of 5 K/h to avoid thermal and time delays [13]. At the end of each measurement, the vessel was dried under vacuum for 24 h to determine the total water content based on the change in mass. Consequently, the amount of water in the vessel was estimated to be in the range of 20.0–25.0 mg. On the other hand, the mass of dried sample in the vessel was in the range of 7.0–8.0 mg in all of the measurements.

4. Results and discussion

4.1. Morphology of the porous structure

Fig. 2 shows the cross section of a RF cryogel synthesized with R/C = 200. A cross section of a typical silica gel (Q-30) is also shown. One can see that the silica gel is composed of spherical particles among which many mesopores are formed. The pore shape factor, F, of the silica gel Q-30 was estimated to be 1.8, which almost coincides with that of the silica gel previously reported by Quinson et al. [9]. The shape factors of the RF hydrogels were determined and are shown in Table 1. Since RF cryogels also possess a porous structure composed of interconnected spherical particles and the pore shape factors of RF cryogel are in fairly good agreement with those of silica

Table 1
Pore shape factors of the samples

Sample	Q-30	RF-200	RF-400	RF-600
F (−)	1.8	1.9	1.9	1.8

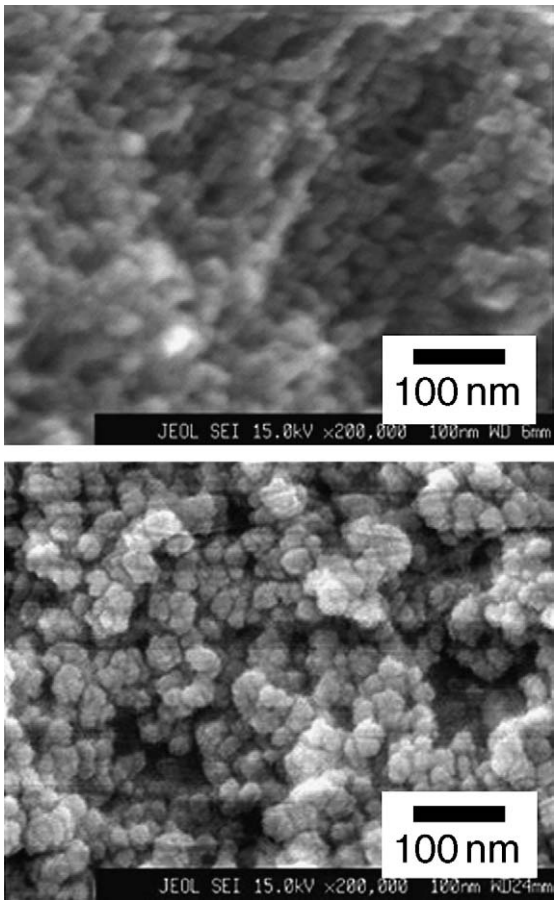

Fig. 2. SEM image of a cross section of RF-200 and Q-30.

gels, it is assumed that the porous structure of RF hydrogels are similar to those of silica gels.

4.2. Evaluation of freezable pore water

Before characterizing the RF hydrogels, the mesoporosity of the silica gel was evaluated. As shown in Fig. 3, this evaluation

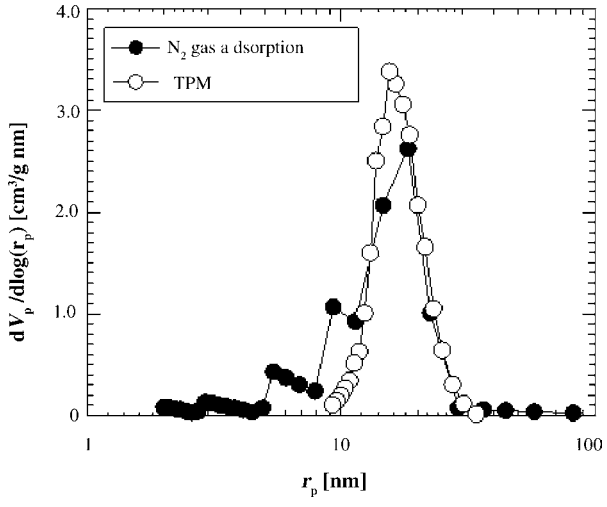

Fig. 3. Pore size distributions of Q-30 assessed by N_2 gas adsorption measurement and TPM.

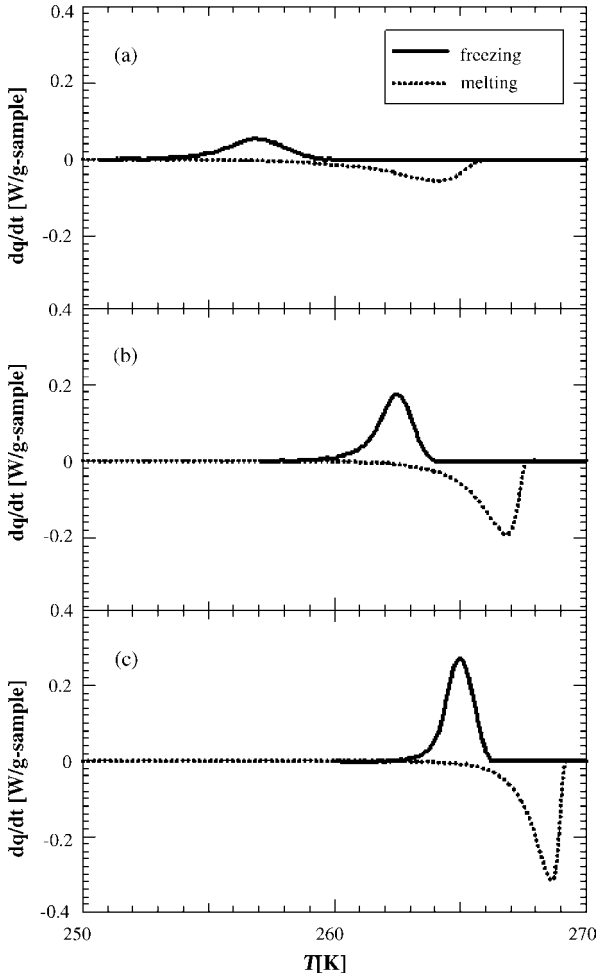

Fig. 4. Thermograms during and freezing and melting of the freezable pore water in RF hydrogels with various pore sizes; (a) RF-200, (b) RF-400, and (c) RF-600.

confirmed a fairly good consistency between the pore size distributions determined by TPM and those measured by the N_2 gas adsorption measurement. Fig. 4 shows the thermograms measured during the freezing and melting of the freezable pore water in the RF hydrogels. In the thermograms of such hydrogels, an exothermic curve attributed to the freezing of the freezable pore water and an endothermic curve corresponding to the melting of the freezable pore water are present. As has been previously reported [15,23], a hysteresis, i.e., an inconsistency between the freezing curve and the melting curve, is clearly observed. As can also be seen in Fig. 4, the peak temperatures of both the freezing curve and the melting curve of the freezable pore water decrease with decreasing R/C value, indicating that the pore size of an RF hydrogel depends on the synthetic conditions of the initial RF solution. This observation will be discussed in more detail in the following section.

4.3. Evaluation of nonfreezable pore water

It was assumed that the BET surface areas of the RF cryogels were considered to be the same as those of the RF hydrogels. Fig. 5 shows the relationship between the BET surface area of an

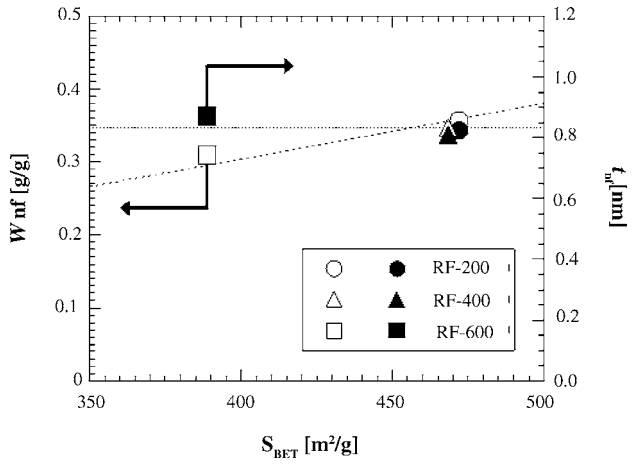

Fig. 5. The relationship between the BET surface area of an RF cryogel and the amount of nonfreezable pore water in an RF hydrogel; broken line: average thickness of the nonfreezable pore water layer, dotted line: linear fit of Eq. (2) relating the BET surface area of an RF cryogel and the amount of nonfreezable pore water in an RF hydrogel.

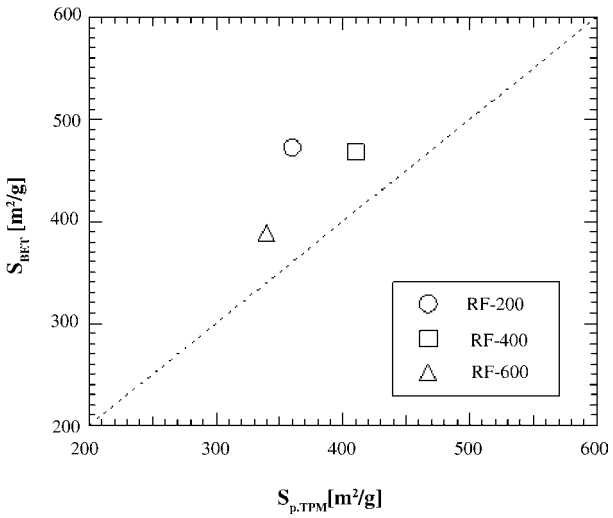

Fig. 7. Comparison of specific surface areas of RF hydrogels and the BET surface area of RF cryogels.

RF cryogel and the amount of nonfreezable pore water. Applying Eq. (2), the thickness of the nonfreezable pore water layers in the RF hydrogels was estimated to be 0.8 nm. These estimated thickness values are close to the value previously reported by Quinson et al. for silica gel beads [9].

4.4. Determination of the porous properties

By using the thickness of the nonfreezable pore water layer estimated in the previous section, the pore size distributions of the RF hydrogels were obtained, as shown in Fig. 6. An RF hydrogel synthesized using $R/W = 500\ \mathrm{kg/m^3}$ was shown to have a narrow size distribution of mesopores. It should be noted that the peak radius of the pore size distribution increased with the increase in R/C, or in other words, with the decrease in the concentration of the basic catalyst for the sol–gel polycondensation. This is because the size of the primary particles that make up the network structure of an RF hydrogel increase with a decrease in the catalyst concentration of the RF solution, as previously reported [7]. As a result of this finding, it is believed that the size of the mesopores formed from the primary particles also decreases. This result clearly indicates that the size of the mesopores of an RF hydrogel can be precisely controlled by varying the amount of catalyst used in the initial RF solution.

The specific surface area, $S_{p,\,TPM}$, of a RF hydrogel and the BET surface area, S_{BET}, of a RF cryogel are compared in Fig. 7. The difference between $S_{p,\,TPM}$ and S_{BET} can be attributed to the assumption in evaluation of t_{nf} using Eq. (2). Another possible reason of the difference is that a RF cryogel possesses a small amount of micropores, which cannot be assessed by TPM. Fig. 8 shows that $S_{p,\,TPM}$ and the volume of mesopores, $V_{p,\,TPM}$, of an RF hydrogel also depend on the R/C ratio. Among the RF hydrogels in this study, RF-400 seems to possess the maximum specific surface area and mesopore volume. These results indicate that both the surface area and the volume of the mesopores of an RF hydrogel can also be changed by adjusting the amount of basic catalyst used in the initial RF solution.

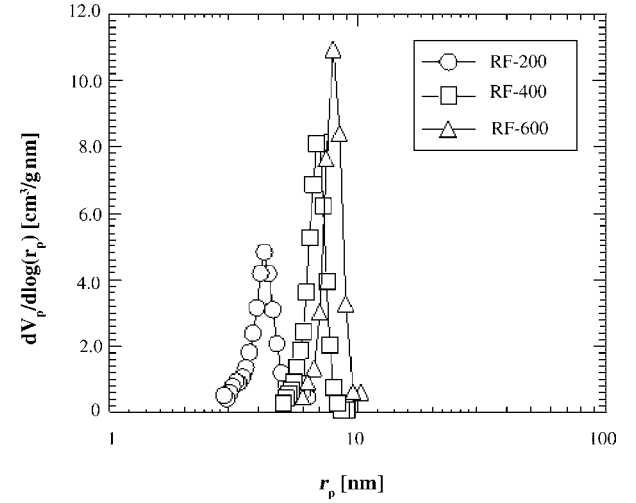

Fig. 6. Pore size distributions of RF hydrogels synthesized by varying the R/C ratio.

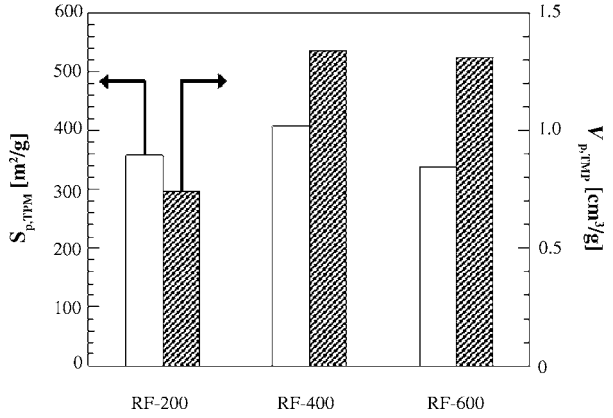

Fig. 8. Specific surface areas and pore volumes of RF hydrogels synthesized by varying the R/C ratio.

5. Conclusions

The effects of the synthetic conditions on the mesoporosity of RF hydrogels, which are synthesized by the sol–gel polycondensation of resorcinol with formaldehyde in a slightly basic aqueous solution, were studied using TPM. Consequently, the relationship between the molar ratio of resorcinol to the basic catalyst (R/C) used in the preparation of the RF solution and the mesoporosity of the resulting RF hydrogel was clarified. The RF hydrogels were confirmed to possess a distribution of mesopores with a fairly uniform size, which could be controlled by adjusting the R/C ratio. The dependencies of both the mesopore volume and surface area of the RF hydrogels on the R/C ratio were also shown.

Acknowledgments

This research was partially supported by The Japan Society for the Promotion of Science, Grant-in-Aid for Scientific Research (B), No. 14350416 (2002), and the Industrial Technology Research Grant Program in 2002 from The New Energy and Industrial Technology Development Organization (NEDO) of Japan.

References

[1] J. Fricke, in: J. Fricke (Ed.), Aerogels, Springer-Verlag, New York, 1986, p. 2.
[2] R.W. Pekala, J. Mater. Sci. 24 (1989) 3221–3227.
[3] R.W. Pekala, C.T. Alviso, F.M. Kong, S.S. Hulsey, J. Non-Cryst. Solids 145 (1992) 90–98.
[4] H. Tamon, H. Ishizaka, M. Mikami, M. Okazaki, Carbon 35 (1997) 791–796.
[5] H. Tamon, H. Ishizaka, T. Araki, M. Okazaki, Carbon 36 (1998) 1257–1262.
[6] H. Tamon, H. Ishizaka, J. Colloid Interface Sci. 206 (1998) 577–582.
[7] T. Yamamoto, T. Yoshida, T. Suzuki, S.R. Mukai, H. Tamon, J. Colloid Interface Sci. 245 (2002) 391–396.
[8] M. Brun, A. Lallemand, J.F. Quinson, C. Eyraud, Thermochim. Acta 21 (1977) 59–88.
[9] J.F. Quinson, J. Dumas, J. Serughetti, J. Non-Cryst. Solids 79 (1986) 397–404.
[10] J.F. Quinson, M. Chatelut, C. Guizard, A. Larbot, L. Cot, J. Non-Cryst. Solids 121 (1990) 72–75.
[11] K. Ishikiriyama, M. Todoki, K. Motomura, J. Colloid Interface Sci. 171 (1995) 92–102.
[12] K. Ishikiriyama, M. Todoki, J. Colloid Interface Sci. 171 (1995) 103–111.
[13] K. Ishikiriyama, M. Todoki, Thermochim. Acta 256 (1995) 213–226.
[14] M.K. Titulaer, M.J. den Exter, H. Talsma, J.B.H. Jansen, J.W. Geus, J. Non-Cryst. Solids 170 (1994) 113–127.
[15] M.K. Titulaer, J.C. van Miltenburg, J.B.H. Jansen, J.W. Geus, Recl. Trav. Chim. Pays-Bas 114 (1995) 361–370.
[16] M. Wulff, Thermochim. Acta 419 (2004) 291–294.
[17] C.T. Kresge, M.E. Leonowicz, W.J. Roth, J.C. Vartuli, J.S. Beck, Nature 359 (1992) 710–712.
[18] S. Inagaki, Y. Fukushima, K. Kuroda, J. Chem. Soc. Chem. Commun. 8 (1993) 680–681.
[19] D. Zhao, Q. Huo, J. Feng, B.F. Chmelka, G.D. Stucky, J. Am. Chem. Soc. 120 (1998) 6024–6036.
[20] R. Denoyel, R.J.M. Pellenq, Langmuir 18 (2002) 2710–2716.
[21] T. Yamamoto, A. Endo, Y. Inagi, T. Ohmori, M. Nakaiwa, J. Colloid Interface Sci. 284 (2005) 614–620.
[22] F. Ehrburger, V. Guérin, J. Lahaye, Colloid. Surface. 14 (1985) 31–45.
[23] A. Schreiber, I. Ketelsen, G.H. Findenegg, Phys. Chem. Chem. Phys. 3 (2001) 1185–1195.